Discontinuous Finite Element S_n Methods on 3-D Unstructured Grids

Todd A. Wareing, John M. McGhee, Jim E. Morel and Shawn D. Pautz

P.O. Box 1663, MS D409

Transport Methods Group, XTM

Los Alamos National Laboratory

Los Alamos, NM 87545

Send proofs and page charges to:

Dr. Todd A. Wareing

Mail Stop D409

Los Alamos National Laboratory

Los Alamos, NM 87545

45 - Pages - 08 Tables - 05 Figures

Abstract

Discontinuous finite element methods for the S_N equations on 3-D unstructured tetrahedral and hexahedral meshes are presented. Solution techniques including source iteration and diffusion-synthetic acceleration are described. Numerical results are presented which demonstrate the accuracy and efficiency of these methods.

I. Introduction

The purpose of this paper is to present methods for solving the S_N equations on 3-D unstructured tetrahedral and hexahedral meshes using the discontinuous finite-element method (DFEM) for the spatial discretization. The majority of DFEMs developed within the reactor physics community have been rectangular-mesh methods. Notable exceptions are the methods used in the TRIPLET[1], TRIDENT[2], and ZEPHYR[3] S_N codes. TRIPLET and TRIDENT are 2-D triangular-mesh codes. Their meshes are actually semi-structured rather than fully unstructured because the triangles are located on bands. The ZEPHYR code has a fully unstructured mesh consisting of arbitrary combinations of quadrilaterals and triangles. There are two significant complications encountered when applying DFEMs to the S_N equations on 2-D unstructured meshes that are not encountered when applying them on 2-D rectangular meshes:

- For quadralaterals, the finite-element matrix elements must be evaluated by quadrature because they cannot be analytically integrated.

- The lower-triangular ordering of the angular flux unknowns required to solve the source iteration equations via the back-substitution or sweeping technique is mesh-dependent. Thus this ordering must be explicitly deter-

mined for each direction via a computational algorithm. On rectangular meshes, this ordering depends upon direction, but it is mesh-independent and trivial to recognize. It has been observed that a lower-triangular ordering exists on all 2-D unstructured meshes as long as the mesh is non-re-entrant as a whole, and each element (spatial cell) within the mesh is non-re-entrant.

Further complications are encountered when DFEMS are applied on 3-D unstructured meshes:

- Because the faces of general hexahedra can be non-planar, a given direction can be incident on one part of a element face and exiting on the other part. This causes the finite-element definition of the angular flux to change on the interior of element faces, whereas such changes never occur with flat faces. These face-interior changes require separate matrix-element integrations within the incident and exiting regions of the face because each region has a different basis function representation for the flux. Since standard finite-element quadratures are intended to integrate a single polynomial flux representation over a whole face, they can be very inaccurate for performing these double-representation integrations. Furthermore, having

directions that are both incident and exiting on the same face make a lower-triangular ordering impossible because the two elements sharing that face become mutually-dependent.

- We initially assumed that if a 3-D unstructured mesh were non-re-entrant as a whole, and if all of the elements in the mesh were non-re-entrant, a lower-triangular ordering of the angular flux unknowns would exist. However, we have found that this is not necessarily true. It is possible for "rings" of mutual dependency to form on 3-D unstructured meshes even if the previously described mesh criteria are met. When this occurs, a lower-triangular ordering of the angular flux unknowns does not exist.

Thus, if one is to develop a DFEM S_N method for 3-D unstructured meshes, one must deal with the complications described above. Our strategy for dealing with them relies on two facts:

- These complications will rarely occur on well-shaped, i.e. not highly skewed, meshes.

- Directions that are both incident and exiting on a face are essentially parallel to the face. Fluxes exactly parallel to to a flat face yield a zero solution within the element. Thus, we expect that such approximations made for

directions nearly parallel to the faces will only weakly affect the overall solution.

The full details are given later, but a high-level description of our strategy can be given as follows:

We deal with a direction that is both incident and exiting on the same face by defining the direction to be either incident or exiting over the whole face via a single average face normal. The finite-element flux representation is then uniquely defined over the entire face. Furthermore, this solves the local problem of mutual coupling between the elements that share the face, but global dependency rings can still form. We use graph theory to identify mutually-dependent rings of elements in the sweep ordering process. The mutual dependence is effectively broken by assuming that the incoming fluxes for one element in the ring are known. This allows the ordering process to continue even though the resulting system of source iteration equations is not lower triangular. Because the equations are not lower triangular, an exact solution is not obtained after each sweep is performed.

The remainder of this paper is organized as follows: in Section II, we describe the DFEM spatial differencing of the S_N equations on 3-D unstructured meshes; in Section III, we describe the solution method for solving these DFEM S_N equations; in Section IV, we present some numerical results; and in Section V we end

with some conclusions.

II. DFEM Spatial Differencing

We first consider the multigroup S_N equations for domain, V, and boundary, δV, and an isotropic fixed source:

$$\underline{\Omega}_m \cdot \underline{\nabla} \Psi_{m,g}(\underline{r}) + \sigma_{t,g}(\underline{r}) \Psi_{m,g}(\underline{r}) = S_{g,m}(\underline{r}) + Q_{g,m}(\underline{r}) \ , \tag{1}$$

$$S_{m,g}(\underline{r}) = \sum_{g=1}^{G} \sum_{l=1}^{L} (2l+1) \sigma_{s,g' \rightarrow g}^{l}(\underline{r}) \sum_{n=-l}^{l} Y_{l,n}(\underline{\Omega}_m) \phi_l^n(\underline{r}) \ , \tag{2}$$

$$\Psi_m(\underline{r}) = F_{m,g}(\underline{r}), \ \underline{n} \cdot \underline{\Omega}_m < 0 \ . \tag{3}$$

Here m and g are the angle and group indices, Ψ is the discrete-ordinate angular flux, F is the incident angular flux, σ_t is the macroscopic total cross section, σ_s is the macroscopic scattering cross section, S is the scattering source represented as an expansion of spherical harmonics ($Y_{l,n}$), Q is the fixed source, and $\underline{n}$ is the outward directed unit normal vector of δV. We need only consider isotropic scattering in the development of the DFEM equations, but this is not a limitation. Expanding the $\underline{\nabla}$ operator using the standard summation convention (i.e. a repeated index in the same multiplicative term implies a summation) and suppressing the

m and g subscripts, Eq.(1) for a single energy group in 3D Cartesian geometry becomes

$$\Omega_i \frac{\partial}{\partial r_i} \Psi(\underline{r}) + \sigma_t(\underline{r}) \Psi(\underline{r}) = \sigma_s(\underline{r}) \Phi(\underline{r}) + Q(\underline{r}) \ , \tag{4}$$

where the individual components of $\underline{\Omega}$ have been written as Ω_i and the individual components of $\underline{\nabla}$ have been written as $\partial/\partial r_i$, where $r_1 = x$, $r_2 = y$ and $r_3 = z$. The indices run from one to the number of spatial dimensions. Unless otherwise noted, this summation convention will be used in all the equations that follow.

A. Discontinuous Finite Element Formulation

We begin the development by assuming that the problem domain has been divided into a unstructured spatial grid of volume elements (spatial cells). The elements shapes are unspecified for now, but we do require that the vertices be connected by straight lines. The material properties within each element are assumed to be constant. The DFEM derivation begins by considering element k, with volume V_k and surface δV_k. We define approximate angular and scalar flux functions within element k in terms of a linearly independent set of basis functions, $[\gamma_p(\underline{r}),\ 1 \leq p \leq P_k]$, where p is the node index and P_k is the number of

nodes per element. These approximate functions take the following form:

$$\Psi(\underline{r}) \cong \psi(\underline{r}) = \underline{\Theta}^T(\underline{r})\underline{\psi} \,, \tag{5}$$

and

$$\Phi(\underline{r}) \cong \phi(\underline{r}) = \underline{\Theta}^T(\underline{r})\underline{\phi} \,, \tag{6}$$

where

$$\underline{\Theta} = \left[\begin{array}{ccc} \gamma_1(\underline{r}), & \cdots, & \gamma_{P_k}(\underline{r}) \end{array} \right]^T \,, \tag{7}$$

$$\underline{\psi} = \left[\begin{array}{ccc} \psi_1, & \cdots, & \psi_{P_k} \end{array} \right]^T \,, \tag{8}$$

and

$$\underline{\phi} = \left[\begin{array}{ccc} \phi_1, & \cdots, & \phi_{P_k} \end{array} \right]^T \,. \tag{9}$$

The basis functions are chosen to give appropriate nodal displacements when the coordinates of corresponding nodes, p, are inserted into Eqs.(5) and (6). That is, $\gamma_p(\underline{r}) = 1$ at $r = (x_p, y_p, z_p)$ and zero at the other nodes. Here $\underline{\psi}$ and $\underline{\phi}$ are column vectors of nodal angular and scalar fluxes, respectively. Next, we apply the Galerkin method, which consists of inserting Eqs. (5)-(6) into Eq. (4), multiplying by $\overrightarrow{\Theta}$ and integrating over V_k. This operation guarantees the orthogonality of the

residuals to the space spanned by the spatial basis functions, thus minimizing, in a certain sense, the error introduced by the approximation introduced in Eq. (5). Carrying out this operation and using the divergence theorem, we obtain:

$$\int_{\delta V_k} \Omega_i n_i \underline{\Theta} \psi^s(\underline{r}) d\delta V - \int_{V_k} \Omega_i \frac{\partial \underline{\Theta}}{\partial r_i} \underline{\Theta}^T \underline{\psi} dV$$

$$+ \int_{V_k} \underline{\Theta} \left\{ \sigma_t \underline{\Theta}^T \underline{\psi} - \sigma_s \underline{\Theta}^T \underline{\phi} - q(\underline{r}) \right\} dV = 0 \ . \tag{10}$$

Here, $n_i(\underline{r})$ is the i-th component of the outward directed unit normal vector to δV and $\psi^s(\underline{r})$ is the angular flux on the element boundary. For each element,

$$\delta V_k = \sum_{l=1}^{N_{faces}} \delta V_{k,l} \ , \tag{11}$$

where l represents the face number and N_{faces} is the total number of faces enclosing element k, for example, $N_{faces} = 4$ for tetrahedral elements and $N_{faces} = 6$ for hexahedral elements To complete the derivation we need to define the element boundary angular fluxes. Here we assign angular flux functions on the upstream side of the boundary as follows:

$$\psi^s(\underline{r}) = \underline{\Theta}^T(\underline{r}) \underline{\psi}^{s,l} \ , \tag{12}$$

where for the l -th face,

$$\underline{\psi}^{s,l} = \begin{array}{l} \underline{\psi} \ , \Omega_i n_i^{av,l} > 0 \\ \underline{\psi}^{inc} \ , \ \Omega_i n_i^{av,l} < 0 \end{array} \ . \tag{13}$$

Here, $\underline{\psi}^{inc}$ is the corresponding column vector of nodal angular flux values of the element that shares the l-th face of element k and $\underline{n}^{av,l}$ is the average unit normal vector of the l-th face, defined by:

$$\underline{n}^{av,l} = \frac{\underline{A}^l}{\| \underline{A}^l \|} \tag{14}$$

where,

$$\underline{A}^l = \int_{\delta V_k} \underline{n}^l d\delta V \ . \tag{15}$$

Equations (13) requires some explanation. For elements with planar faces (tetrahedra) these definitions are consistent with the finite-element formalism. For non-planar faces, the unit normal vector to the face is not constant across the face and a given direction can be both incident and exiting to the face. This results in a mutual dependency between the elements that share the face and thereby makes a lower triangular ordering impossible. If the unit normal vector to a face does not change sign then the use of an average normal for defining incident and exiting fluxes remains fully consistent with the finite-element formalism. If the unit normal vector to a face does change sign we define each given direction to either be incident or exiting across the entire face based upon the average outward directed unit normal vector to the face. This is not consistent with the finite-element formalism and therefore represents an additional approximation.

The DFEM equations for each element are then given by:

$$\sum_{l=1}^{N_{faces}} \Omega_i \underline{\underline{U}}_i^l \underline{\psi}^{s,l} + \left(-\Omega_i \underline{\underline{K}}_i + \sigma_t \underline{\underline{M}} \right) \underline{\psi} = \sigma_s \underline{\underline{M}}\, \underline{\phi} + \underline{q} \ , \tag{16}$$

where,

$$\underline{\underline{U}}_i^l = \int_{\delta V_{k,l}} n_i \underline{\Theta}\, \underline{\Theta}^T \, d\delta V \ , \tag{17}$$

$$\underline{\underline{K}}_i = \int_{V_k} \frac{\partial \underline{\Theta}}{\partial r_i} \underline{\Theta}^T dV \ , \tag{18}$$

$$\underline{\underline{M}} = \int_{V_k} \underline{\Theta}\, \underline{\Theta}^T dV \ , \tag{19}$$

$$\underline{q} = \int_{V_k} \underline{\Theta} q(\underline{r}) dV \ . \tag{20}$$

B. Spatial Derivatives and Integrals

In general the volume elements will be non-orthogonal and it becomes necessary to transform from global coordinates, $\underline{r} = (x, y, z)$, with difficult limits of integration, to local coordinates, $\underline{\widetilde{r}} = (\widetilde{x}, \widetilde{y}, \widetilde{z},$ with simple limits of integration. The local coordinate system is defined such that the physical cell takes on a simple shape and size. For example, every hexahedral is a unit cube in the local

coordinate system. The most convenient method of establishing the coordinate transformations is to use the local basis functions to represent the variation of the unknown coordinate. If, for instance, we write for each element:

$$x(\underline{\tilde{r}}) = \underline{\Theta}^T(\underline{\tilde{r}}) \begin{bmatrix} x_1 \\ \vdots \\ x_{P_k} \end{bmatrix} = \underline{\Theta}^T(\underline{\tilde{r}})\underline{x} \ , \tag{21}$$

$$y(\underline{\tilde{r}}) = \underline{\Theta}^T(\underline{\tilde{r}}) \begin{bmatrix} y_1 \\ \vdots \\ y_{P_k} \end{bmatrix} = \underline{\Theta}^T(\underline{\tilde{r}})\underline{y} \ , \tag{22}$$

$$z(\underline{\tilde{r}}) = \underline{\Theta}^T(\underline{\tilde{r}}) \begin{bmatrix} z_1 \\ \vdots \\ z_{P_k} \end{bmatrix} = \underline{\Theta}^T(\underline{\tilde{r}})\underline{z} \ , \tag{23}$$

where, $\underline{y}$, $\underline{z}$ are column vectors of the nodal coordinates, immediately a relationship of the required form is available. It is necessary to have some means of expressing the global spatial derivatives in terms of local derivatives. This is done in the literature[4] and only the final result is given. Thus,

$$dV = dxdydz = \det \mathcal{J}(\underline{\tilde{r}}) d\tilde{x}d\tilde{y}d\tilde{z} = \det \mathcal{J}(\underline{\tilde{r}}) d\tilde{V} \tag{24}$$

$$\frac{\partial}{\partial r_i} = \mathcal{J}^{-1}_{i,j}(\widetilde{\underline{r}}) \frac{\partial}{\partial \widetilde{r}_j} \ , \tag{25}$$

where $\mathcal{J}$ is the Jacobian matrix defined by:

$$\mathcal{J}(\widetilde{\underline{r}}) = \begin{bmatrix} \left(\frac{\partial \underline{\underline{\Theta}}^T}{\partial \widetilde{x}} \underline{x}\right) & \left(\frac{\partial \underline{\underline{\Theta}}^T}{\partial \widetilde{x}} \underline{y}\right) & \left(\frac{\partial \underline{\underline{\Theta}}^T}{\partial \widetilde{x}} \underline{z}\right) \\ \left(\frac{\partial \underline{\underline{\Theta}}^T}{\partial \widetilde{y}} \underline{x}\right) & \left(\frac{\partial \underline{\underline{\Theta}}^T}{\partial \widetilde{y}} \underline{y}\right) & \left(\frac{\partial \underline{\underline{\Theta}}^T}{\partial \widetilde{y}} \underline{z}\right) \\ \left(\frac{\partial \underline{\underline{\Theta}}^T}{\partial \widetilde{z}} \underline{x}\right) & \left(\frac{\partial \underline{\underline{\Theta}}^T}{\partial \widetilde{z}} \underline{y}\right) & \left(\frac{\partial \underline{\underline{\Theta}}^T}{\partial \widetilde{z}} \underline{z}\right) \end{bmatrix} \ . \tag{26}$$

For the boundaries we have:

$$d\delta V = \left|\mathcal{J}_s(\widetilde{\underline{r}}_s)\right| d\widetilde{x}_s d\widetilde{y}_s = \left|\mathcal{J}_s(\widetilde{\underline{r}}_s)\right| d\delta \widetilde{V} \ , \tag{27}$$

where the $\widetilde{x}_s$ and $\widetilde{y}_s$ coordinates are assumed to be the local coordinates for the element face, $|\mathcal{J}_s|$ is the magnitude of the surface Jacobian given by:

$$\mathcal{J}_s(\widetilde{\mathbf{r}}_s) = \begin{bmatrix} \left(\frac{\partial \underline{\underline{\Theta}}^T}{\partial \widetilde{x}_s} \underline{x}\right) \\ \left(\frac{\partial \underline{\underline{\Theta}}^T}{\partial \widetilde{x}_s} \underline{y}\right) \\ \left(\frac{\partial \underline{\underline{\Theta}}^T}{\partial \widetilde{x}_s} \underline{z}\right) \end{bmatrix} \times \begin{bmatrix} \left(\frac{\partial \underline{\underline{\Theta}}^T}{\partial \widetilde{y}_s} \underline{x}\right) \\ \left(\frac{\partial \underline{\underline{\Theta}}^T}{\partial \widetilde{y}_s} \underline{y}\right) \\ \left(\frac{\partial \underline{\underline{\Theta}}^T}{\partial \widetilde{y}_s} \underline{z}\right) \end{bmatrix} \ . \tag{28}$$

Equations (17) - (20) become:

$$\underline{\underline{U}}^l_i = \int_{\delta \widetilde{V}_{k,l}} n_i \underline{\underline{\Theta}}\, \underline{\underline{\Theta}}^T \left|\mathcal{J}_s(\widetilde{\underline{r}}_s)\right|_l d\delta \widetilde{V}, \tag{29}$$

$$\underline{\underline{K}}_i = \int_{\widetilde{V}_k} \mathcal{J}^{-1}_{i,j}(\widetilde{\mathbf{r}}) \frac{\partial \underline{\underline{\Theta}}}{\partial \widetilde{r}_j} \underline{\underline{\Theta}}^T \det \mathcal{J}(\widetilde{\underline{r}}) d\widetilde{V} \ , \tag{30}$$

$$\underline{\underline{M}} = \int_{\widetilde{V}_k} \underline{\Theta}\,\underline{\Theta}^T \det \mathcal{J}\,(\underline{\widetilde{r}}) d\widetilde{V}\ , \tag{31}$$

$$\underline{q} = \int_{\widetilde{V}_k} \underline{\Theta} q(\underline{\widetilde{r}}) \det \mathcal{J}\,(\underline{\widetilde{r}}) d\widetilde{V}\ . \tag{32}$$

Because the limits of integration are fixed, we can perform these integrals with sufficient accuracy using Gauss quadrature.

III. Solution Technique

The DFEM equations are solved using source iteration (SI) in conjunction with diffusion-synthetic acceleration (DSA), as described by the following equations:

$$\underline{\Omega} \cdot \underline{\nabla} \Psi^{(\ell+1/2)} + \sigma_t \Psi^{(\ell+1/2)} = \sigma_s \Phi^{(\ell)} + Q, \tag{33}$$

$$-\underline{\nabla} \cdot \frac{1}{3\sigma_t} \underline{\nabla} \delta\Phi^{(\ell+1)} + \sigma_a \delta\Phi^{(\ell+1)} = \sigma_s \left(\Phi^{(\ell+1/2)} - \Phi^{(\ell+1)} \right), \tag{34}$$

$$\Phi^{(\ell+1)} = \Phi^{(\ell+1/2)} + \delta\Phi^{(\ell+1)}. \tag{35}$$

Here, ℓ is the iteration index. Equation (33) is the sweep equation and Eq. (34) is the DSA equation.

A. Source Iteration and Transport Sweeps

The discretization of Eq.(33) in angle and space yields, for each angle in the discrete set, a system of equations whose associated matrix can be written in block lower triangular form (the sweep matrix), where each block is usually associated with the unknowns in a single spatial element. The dependencies between the elements for any angle can also be expressed in terms of a directed graph. If this sweep graph is acyclic, then each of the blocks in the matrix is associated with a single element; if the graph is cyclic then at least one of the blocks is associated with more than one element. In the latter case, the source iteration equations can no longer be exactly solved using a sweep.

Each system of DFEM S_N equations is solved by the method of sweeping. The spatial elements are placed into an ordered list in which the order results in a block lower triangular matrix. Each block is solved in succession. Physically this solution order resembles a wave front propagating through the mesh roughly in the direction of the associated angle. In the case of a cyclic sweep graph a depth first search algorithm[5] is used to determine the identities of the elements in each cycle (associated with a large block in the matrix). These cycles are "broken" by approximating one or more unknown incoming face fluxes with the values from the previous source iteration; this approximation yields a modified sweep matrix

in which each block refers to the unknowns of only one element.

Although most of the smooth meshes we have generated and examined have yielded only directed acyclic sweep graphs, we have observed cyclic graphs in both tetrahedral and hexahedral meshes. The use of previous iterate information has not noticeably degraded the performance or stability of the SI or DSA iterations. Presently, our algorithm for breaking the cycles has not been optimized, thus, if many cycles are present, a dramatic increase in run time can be expected.

B. Acceleration Equations

Specific details of DSA are widely available in the literature[6,7]. One very important and well known fact about DSA is that the discretization of Eq.(34) must be consistent (or nearly consistent) with the discretization of Eq.(33). The four-step method[7] is one way to obtain completely consistent differencing of Eq.(34) for all differencing schemes, but for advanced differencing schemes such as DFEMs in multidimensions, the resulting P_1 system of equations cannot be collapsed into a single discretized diffusion equation. Adams and Martin have proposed a "modified four-step" DSA method[8] for DFEMs, where the diffusion differencing is obtained by applying a DFEM method to the diffusion equation. Their method leads to a single discretized diffusion equation, which is both non-

standard and non-symmetric . Both the four-step and modified four-step methods are stable and effective for DFEMs, but the resulting equations are difficult to solve in an efficient manner on unstructured meshes. Wareing, Larsen and Adams[9] have developed yet another approach for obtaining nearly consistent DSA equations for DFEMs. This approach leads to a discretized diffusion equation that can be solved very efficiently, however, although the method is always stable, the effectiveness is significantly degraded for skewed and high aspect ratio elements. We use an adaptation of Wareing, Larsen and Adams method.

To derive the discretization of Eq.(34), using an adaptation of the Wareing, Larsen and Adams method, we begin by defining approximate scalar flux correction functions within element k in terms of the same linearly independent set of basis functions that we used with the discrete-ordinate equations:

$$\delta\Phi(\underline{r}) \cong \delta\phi(\underline{r}) = \underline{\Theta}^T(\underline{r})\underline{\delta\phi} \ . \tag{36}$$

If we multiply Eq.(34) by $\underline{\Theta}$, integrate over the volume V, and insert Eq.(36) into the resulting equations, we obtain:

$$-\sum_{l=1}^{N_{faces}} \frac{1}{3\sigma_t}\int_{\delta V_{k,l}} n_i^l \underline{\Theta}\frac{\partial}{\partial r_i}\delta\phi^{s,(\ell+1)}(\underline{r})d\delta V + \frac{1}{3\sigma_t}\int_{V_k}\left(\frac{\partial\underline{\Theta}}{\partial r_i}\right)\left(\frac{\partial\underline{\Theta}^T}{\partial r_j}\right)\underline{\delta\phi}^{(\ell+1)}dV$$

$$+\int_{V_k}\underline{\Theta}\left\{\sigma_a\underline{\Theta}^T\underline{\delta\phi}^{(\ell+1)} - \sigma_s\underline{\Theta}^T\left(\underline{\phi}^{(\ell+1/2)} - \underline{\phi}^{(\ell)}\right)\right\}dV = 0 \ . \tag{37}$$

All that is needed at this point is the definition of $\delta\phi^{s,(\ell+1)}(\underline{r})$, the scalar flux corrections on the boundary of the element. In the modified four-step method of Adam and Martin, one uses the partial current approach to define for the l-th face:

$$-\frac{n_i^l}{3\sigma_t}\frac{\partial}{\partial r_i}\delta\phi^{s,(\ell+1)}(\underline{r}) = \left\{\frac{\underline{\Theta}^T\underline{\delta\phi}^{(\ell+1)}}{4} - \frac{n_i^l}{6\sigma_t}\frac{\partial\underline{\Theta}^T}{\partial r_i}\underline{\delta\phi}^{(\ell+1)}\right\}$$

$$-\left\{\frac{\underline{\Theta}^T\underline{\delta\phi}^{inc,(\ell+1)}}{4} + \frac{n_i^l}{6\sigma_t}\frac{\partial\underline{\Theta}^T}{\partial r_i}\underline{\delta\phi}^{inc,(\ell+1)}\right\} \ . \qquad (38)$$

Here, $\underline{\delta\phi}^{inc,(l+1)}$, is the corresponding column vector of nodal scalar flux correction values of the element that shares the l-th face of element k. This leads to a nonsymmetric DFEM for the diffusion equation that is nonstandard and cannot be solved efficiently with standard solvers. To simplify these equations, suppose we assume the scalar flux corrections are continuous at the interelement boundaries and set $\underline{\delta\phi}^{(\ell+1)} = \underline{\delta\phi}^{inc,(\ell+1)} = \underline{\delta\phi}^{(\ell+1)}_{cont}$ in Eq.(38), then Eq.(37) becomes:

$$-\sum_{l=1}^{N_{faces}}\frac{1}{3\sigma_t}\int_{\delta V_{k,l}} n_i^l\underline{\Theta}\frac{\partial\underline{\Theta}^T}{\partial r_i}\underline{\delta\phi}^{(\ell+1)}_{cont}d\delta V + \frac{1}{3\sigma_t}\int_{V_k}\left(\frac{\partial\underline{\Theta}}{\partial r_i}\right)\left(\frac{\partial\underline{\Theta}^T}{\partial r_j}\right)\underline{\delta\phi}^{(\ell+1)}_{cont}dV$$

$$+\int_{V_k}\underline{\Theta}\left\{\sigma_a\underline{\Theta}^T\underline{\delta\phi}^{(\ell+1)}_{cont} - \sigma_s\underline{\Theta}^T\left(\underline{\phi}^{(\ell+1/2)} - \underline{\phi}^{(\ell)}\right)\right\}dV = 0 \ . \qquad (39)$$

These equations represent the contribution from element k to the individual vertices forming element k. A global CFEM matrix is formed for all vertices in the mesh by summing the individual element contributions using the standard finite-element technique[4]. This global matrix is a N_{vertex} x N_{vertex} symmetric positive-definite matrix, where N_{vertex} is the number of vertices in the mesh. Marshak

boundary conditions are used for all boundary vertices. If one uses the CFEM differencing solely for the DSA equations, that is, assign the discontinuous scalar flux correction to the continuous scalar flux correction, the resulting method is stable but becomes ineffective for optically thick cells.

In the method of Wareing, Larsen and Adams, the CFEM differencing is used in conjunction with a local mapping from continuous scalar flux corrections to discontinuous scalar flux corrections. We use an adaptation of this method, where this mapping is derived from the modified four-step method by assuming for the l-th face that

$$\frac{\underline{\Theta}^T \underline{\delta\phi}^{(\ell+1)}_{cont}}{2} = \left\{ \frac{\underline{\Theta}^T \underline{\delta\phi}^{(\ell+1)}}{4} - \frac{n_i^l}{6\sigma_t} \frac{\partial \underline{\Theta}^T}{\partial r_i} \underline{\delta\phi}^{(\ell+1)} \right\}$$

$$+ \left\{ \frac{\underline{\Theta}^T \underline{\delta\phi}^{inc,(\ell+1)}}{4} + \frac{n_i^l}{6\sigma_t} \frac{\partial \underline{\Theta}^T}{\partial r_i} \underline{\delta\phi}^{inc,(\ell+1)} \right\} \ . \tag{40}$$

Note that Eq.(40) represents a discontinuous variation on the P_1 identity, $\phi/2 = (\underline{J}^+ + \underline{J}^-)$. Eq.(38) then becomes:

$$-\frac{n_i^l}{3\sigma_t} \frac{\partial}{\partial r_i} \delta\phi^{s,(\ell+1)}(\underline{r}) = \left\{ \frac{\underline{\Theta}^T \underline{\delta\phi}^{(\ell+1)}}{2} - \frac{n_i^l}{3\sigma_t} \frac{\partial \underline{\Theta}^T}{\partial r_i} \underline{\delta\phi}^{(\ell+1)} \right\}$$

$$- \frac{\underline{\Theta}^T \underline{\delta\phi}^{(\ell+1)}_{cont}}{2} \ . \tag{41}$$

Inserting Eq.(41) into Eq.(37), results in the following local set of equations (P_k unknowns) for element k that are de-coupled from all other elements:

$$\sum_{l=1}^{N_{faces}} \int_{\delta V_{k,l}} \underline{\Theta} \left(\frac{\underline{\Theta}^T \underline{\delta\phi}^{(\ell+1)}}{2} - \frac{\underline{\Theta}^T \underline{\delta\phi}_{cont}^{(\ell+1)}}{2} \right) d\delta V$$

$$- \sum_{l=1}^{N_{faces}} \frac{1}{3\sigma_t} \int_{\delta V_{k,l}} n_i^l \underline{\Theta} \frac{\partial \underline{\Theta}^T}{\partial r_i} \underline{\delta\phi}^{(\ell+1)} d\delta V + \frac{1}{3\sigma_t} \int_{V_k} \left(\frac{\partial \underline{\Theta}}{\partial r_i} \right) \left(\frac{\partial \underline{\Theta}^T}{\partial r_i} \right) \underline{\delta\phi}^{(\ell+1)} dV$$

$$+ \int_{V_k} \underline{\Theta} \left\{ \sigma_a \underline{\Theta}^T \underline{\delta\phi}_{cont}^{(\ell+1)} - \sigma_s \underline{\Theta}^T \left(\underline{\phi}^{(\ell+1/2)} - \underline{\phi}^{(\ell)} \right) \right\} dV = 0 \ . \qquad (42)$$

For elements with a constant Jacobian (such as tetrahedra),

$$\frac{1}{3\sigma_t} \int_{V_k} \left(\frac{\partial \underline{\Theta}}{\partial r_i} \right) \left(\frac{\partial \underline{\Theta}^T}{\partial r_i} \right) \underline{\delta\phi}^{(\ell+1)} dV$$

$$- \sum_{l=1}^{N_{faces}} \frac{1}{3\sigma_t} \int_{\delta V_{k,l}} n_i^l \underline{\Theta} \frac{\partial \underline{\Theta}^T}{\partial r_i} \underline{\delta\phi}^{(\ell+1)} d\delta V = 0 \ , \qquad (43)$$

and Eq.(42) becomes

$$\sum_{l=1}^{N_{faces}} \int_{\delta V_{k,l}} \underline{\Theta} \left(\frac{\underline{\Theta}^T \underline{\delta\phi}^{(\ell+1)}}{2} - \frac{\underline{\Theta}^T \underline{\delta\phi}_{cont}^{(\ell+1)}}{2} \right) d\delta V$$

$$+ \int_{V_k} \underline{\Theta} \left\{ \sigma_a^{(\ell+1)} \underline{\Theta}^T \underline{\delta\phi}^{(\ell+1)} - \sigma_s \underline{\Theta}^T \left(\underline{\phi}^{(\ell+1/2)} - \underline{\phi}^{(\ell)} \right) \right\} dV = 0 \ . \qquad (44)$$

Although Eq.(43) does not hold for non-orthogonal hexahedral grids (element with non-constant jacobians), we assume that it does. Therefore, given $\underline{\delta\phi}_{cont}^{(\ell+1)}$, the

CFEM scalar flux corrections, a reasonable approximation of $\underline{\delta\phi}^{(\ell+1)}$, the DFEM scalar flux corrections, can be easily obtained from Eq.(44).

We have performed a Fourier analysis for our DSA method on orthogonal hexahedral meshes and have found that for cube meshes the spectral radius approaches a maximum of 0.83 for optically thick elements with a scattering ratio equal to unity and zero for optically thick elements with scattering ratios less than unity. As in the method of Wareing, Larsen and Adams, the performance of the DSA method degrades as the aspect ratio of the elements become large. Later in the paper we provide numerical results to demonstrate the effectiveness of the DSA method on unstructured grids.

IV. Numerical Results

A. Mesh Anomalies

In this section we show, for two different hexahedral meshes, the number of "rings" of mutual dependency, as discussed in the previous sections, as well as the number of faces that are both incoming and exiting for a given angle. The first mesh, as show in Figure (1), is generated from a cube of (20x20x20) orthogonal hexahedral elements. The mesh elements are made non-orthogonal by perturb-

ing the element widths using pseudo-random numbers. In particular, each vertex (except the first and last) is given a perturbed coordinate as follows:

$$z_p = z_u + 0.15\Delta x_u(2R_a - 1) \ ,$$

where z_p denotes the unperturbed element width, z_u denotes the unperturbed coordinate, Δx_udenotes the unperturbed element width, and R_a denotes a pseudo-random number. The average element edge width is approximately the same as that for the orthogonal mesh. This type of mesh is not a smooth mesh and not representative of a "quality" hexahedral mesh.

The second mesh, as show in Figure (2), is a sphere comprised of non-orthogonal elements and was generated using ICEM Hexa^{TM}, a commercial grid generator. This mesh is smooth and is representative of a "quality" hexahedral mesh.

In Table I and II we provide for the smooth and non-smooth meshes, repectively, the number of faces that are both incoming and exiting for a given angle (and a percentage of the total face-angle combinations) for a given S_N order as well as the number of "rings" of mutual dependency. Here we see that both the percentage of the faces that are both incoming and exiting for a given angle and number of rings of mutual dependency is much larger for the non-smooth mesh than that from the smooth mesh. We note that our algorithm for breaking the "rings" of mutual dependency is not optimized, therefore, for problems with a

large number of these rings, the total computational time can be significantly increased.

B. Accuracy

1. Test Problem One

The first test problem is designed to compare the accuracy of the DFEMs on unstructured tetrahedral meshes and hexahedral meshes. This test problem consists of a 1-D homogeneous slab of isotropically-scattering material with a total length of 1 cm, a total cross section of 2 cm^{-1}, a scattering ratio of 0.5, a spatially-constant isotropic homogeneous source of 1 $\frac{particle}{cm^3-s}$, and vacuum boundaries. Obviously, no analytic solution exists for this problem, therefore, we use a highly refined slab geometry S_{16} solution using Gauss-Legendre quadrature as a reference solution. The problem is modeled in 3-D with reflecting boundaries on each boundary perpendicular to the y and z axes. Tchebyschev-Legendre S_{16} quadrature is chosen so that the Legendre angular cosines correspond to the x axis, therefore, the converged 3-D solution will equal that of the 1-D solution.

Calculations were performed on a sequence of four tetrahedral grids, four orthogonal hexahedral grids and four non-orthogonal hexahedral grids. The four

tetrahedra meshes, as described in Table (III), are unstructured but similar in all respects other than number and size of the tetrahedral elements. The four orthogonal and non-orthogonal hexahedral mesh sequences use 5, 10, 20 and 40 elements per side of a 1 cm single material cube. The non-orthogonal meshes begin with the orthogonal mesh, but the widths are perturbed using pseudo-random numbers, as discussed in the previous section.

The absolute value of the relative error in the total absorption rate as a function of average element edge width is plotted in Figure (3) for the tetrahedral, orthogonal hexahedral and non-orthogonal hexahedral grid solutions. All of the solutions exhibit third-order accuracy, even for non-orthogonal hexahedral meshes which contain several faces that are both incoming and exiting for a given angle. We note that the non-orthogonal mesh with 20 elements per side is identical the the mesh in the previous section which has a considerable number dependency rings and faces that are both incoming and exiting for a given angle. We also note that these anomalies had no effect on the iterative solution technigue.

C. Acceleration

1. Test Problem Two

The second test problem is designed to show the effectiveness of the DSA method with tetrahedral meshes and non-orthogonal hexahedral meshes with and without degenerate elements. A degenerate element is formed when one or more vertices have the same coordinates. The problem consists of a homogeneous sphere with vacuum boundary conditions. We vary the total cross section and the scattering ratio. The tetrahedral mesh consists of 607 tetrahedra with an average element edge width of 0.259 cm. The hexahedral mesh without degeneracies consists of 648 hexahedra with an average element edge width of 0.317 cm. The hexahedral mesh with degeneracies (some of the hexahedra have degenerated into tetrahedra, wedges and pyramids) consists of 576 hexahedra.

The spectral radii for each mesh as a function of total cross section and scattering ratio is given in Tables (IV),(V) and (VI) for the tetrahedral mesh, hexahedral mesh without degeneracies and hexahedral mesh with degeneracies respectively. The spectral radii for a small total cross section are small because of the large amount of leakage.

Here we see that the DSA method is very effective under most conditions.

For the tetrahedral mesh and hexahedral mesh without degeneracies, we see that the spectral radii degrades as $c \rightarrow 1$ and as σ_t becomes large. Clearly this effect is more pronounced for the hexadedral mesh with degeneracies. With increasing amounts of absorption, this degradation in the spectral radii diminishes. These results demonstrate that the DSA method should be very effective for most neutronic problems provided the elements are not too skewed, but may be inadequate for radiative transfer problems.

2. Test Problem Three

This problem is designed to show the efficiency of the DSA method on a heterogeneous test problem. The problem is a sphere with a diameter of 2.0 cm containing a 1.0 cm x 1.0 cm x 1.0 cm cube in the center. The sphere has a total cross section in of 10 $cm^{-1}$and the scattering ratio is unity. The total cross section in the box, $\sigma_{t,box}$, is set to $0.01 cm^{-1}$,1.0 cm^{-1} or 10.0 cm^{-1} and the scattering ratio is 0.9. There is a homogeneous source of strength 1 $\frac{particle}{cm^3-s}$ inside the box. The problem is solved on an unstructured tetrahedral mesh and a hexahedral mesh without degeneracies. The tetrahedral mesh contains 1735 elements and is shown if Figure (4). The hexahedral mesh contains 2016 elements and is shown in Figure (5). The problem was solved with S_4 level-symmetric quadrature with a

convergence criterion of 10^{-4}.

Tables (VII) and (VIII) give the SI and DSA CPU time and number of transport iterations for the tetrahedral and hexahedral meshes, respectively. The absorption rate percentage is given to verify that the two element mesh types are giving the same answer. Here we see that the DSA method is very effective and efficient for this problem. The DSA method is very efficient and only increases the time per iteration by about 6 percent.

V. Conclusions

We have successfully developed and implimented discontinuous finite element methods for the S_N equations on 3-D unstructured tetrahedral and hexahedral grids. We have discussed the difficulties involved in developing these methods and acceptable techniques for dealing with them. We have demonstrated that the DFEM's are third order accurate for the scalar fluxes on both tetrahedral meshes and on non-orthogonal hexahedral meshes even with the presense of faces that are both incoming and exiting for a given angle. The source iterations have successfully been accelerated with a DSA method that is efficient and effective for most types of problems, especially neutronics problems. We are presently investigating other DSA techniques that are effective for all types of problems, especially ther-

mal radiative transfer problems. Finally, we plan to optimize our algorithm for breaking the “rings” of mutual dependency described in previous sections.

Acknowledgments

This work was performed under the auspices of the United States Department of Energy.

References

[1]Reed, W. H. et al., “TRIPLET: A Two-Dimensional, Multigroup, Triangular-Mesh, Planar Geometry, Explicit Transport Code,”. Los Alamos Scientific Laboratory Report LA-5428-MS, (1973).

[2]Seed, T. J. et al., “TRIDENT: A Two-Dimensional, Multigroup, Triangular-Mesh, Planar Geometry, Explicit Transport Code,”Los Alamos Scientific Laboratory Report LA-6735-MS, (1977).

[3]Mordant, M., “Some Efficient Lagrangian Mesh Finite Elements Encoded in ZEPHYR for Two Dimensional Transport Calculations,”*Annals of Nuclear Energy*, 18, 609 (1981).

[4]Zienkiewicz, O.C. and Taylor, R.L., *The Finite Element Method*, Fourth Edition, Volume 1, McGraw-Hill Book Company, (1994).

[5]Aho, A.V., Hopcroft, J.E. and Ullman, J.D., *The Design and Analysis of Computer Algorithms*, Addison-Wesley, Reading, MA (1974).

[6]Alcouffe, R.E. “Diffusion Synthetic Acceleration Methods for the Diamond Differenced Discrete Ordinate Equations,” *Nucl. Sci. Eng.*, 66**,** 344 (1977).

[7]Larsen, E.W. “Unconditionally Stable Diffusion Synthetic Acceleration Methods for the Slab Geometry Discrete Ordinates Equations Part1: Theory,” *Nucl. Sci. Eng.*, 82**,** 47 (1982).

[8]Adams, M.L. and Martin, W.R. “Diffusion Synthetic Acceleration of Discontinuous Finite Element Transport Iterations,” *Nucl. Sci. Eng.*, 111**,** 145 (1992).

[9]Wareing, T.A., Larsen, E.W. and Adams, M.L., “Diffusion Accelerated Discontinuous Finite Element Schemes for the S_N Equations in Slab and X-Y Geometries.,” Proc. Int. Topl. Mtg on Advances in Mathematics, Computations and Reactor Physics, Pittsburg, PA., USA, April 29 - May 2, 1991, American Nuclear Society (1991)

Table I: Dependency Rings and Re-entrant Faces For Cube of Random Hexahedral Elements

S_N Order (angles)	Re-entrant Faces (Percentage)	Dependency Rings
2 (8)	0 (0.00)	0
4 (24)	4 (0.0002)	0
6 (48)	9,084 (0.30)	0
8 (80)	73,372 (1.45)	36
10 (120)	207,432 (2.70)	316
12 (168)	369,540 (3.44)	952
14 (224)	543,980 (3.79)	1,790
16 (288)	721,544 (3.91)	2,664

Table II: Dependency Rings and Re-entrant Faces For Sphere of Hexahedral Elements

S_N Order (angles)	Re-entrant Faces (Percentage)	Dependency Rings
2 (8)	928 (0.22)	0
4 (24)	3,884 (0.30)	0
6 (48)	4,492 (0.18)	0
8 (80)	9,970 (0.23)	0
10 (120)	11,458 (0.18)	0
12 (168)	19,080 (0.21)	0
14 (224)	24,192 (0.20)	0
16 (288)	29,282 (0.19)	4

Table III: Tetrahedral Mesh Description for Test Problem Two.

Mesh ID	Tetrahedra	Average Cell Edge Width (mfp)
1	192	0.7070
2	1536	0.3536
3	12228	0.1770
4	98304	0.0884

Table IV: Spectral Radius for Test Problem Two Using Tetrahedral Mesh.

σ_t	$c = 1.00$	$c = 0.99$	$c = 0.90$
0.1	0.03	0.03	0.03
1.0	0.17	0.17	0.15
10.0	0.58	0.57	0.49
100.0	0.90	0.87	0.61
1000.0	0.95	0.71	0.25

Table V: Spectral Radius for Test Problem Two Using Hexahedral Mesh Without Degenerate Elements.

σ_t	$c = 1.00$	$c = 0.99$	$c = 0.90$
0.1	0.03	0.03	0.03
1.0	0.17	0.17	0.15
10.0	0.36	0.36	0.32
100.0	0.68	0.64	0.54
1000.0	0.86	0.72	0.35

Table VI: Spectral Radius for Test Problem Two Using Hexahedral Mesh With Degenerate Elements.

σ_t	$c = 1.00$	$c = 0.99$	$c = 0.90$
0.1	0.05	0.05	0.05
1.0	0.27	0.27	0.23
10.0	0.75	0.74	0.63
100.0	1.00	0.99	0.87
1000.0	1.00	0.99	0.71

Table VII: Tetrahedral Mesh CPU time and Iteration Counts for Test Problem Three.

	SI		DSA		
$\sigma_{t,box}$	CPU Time	Iters	CPU Time	Iters	Abs. Rate (%)
0.1	573.8	157	57.9	15	1.276
1.0	558.0	153	45.8	12	11.78
10.0	496.7	136	35.0	9	62.10

Table VIII: Hexahedral Mesh CPU time and Iteration Counts for Test Problem Three.

	SI		DSA		
$\sigma_{t,box}$	CPU Time	Iters	CPU Time	Iters	Abs. Rate (%)
0.1	1863.8	157	118.1	9	1.277
1.0	1822.5	153	105.0	8	11.79
10.0	1619.3	137	79.7	6	62.17

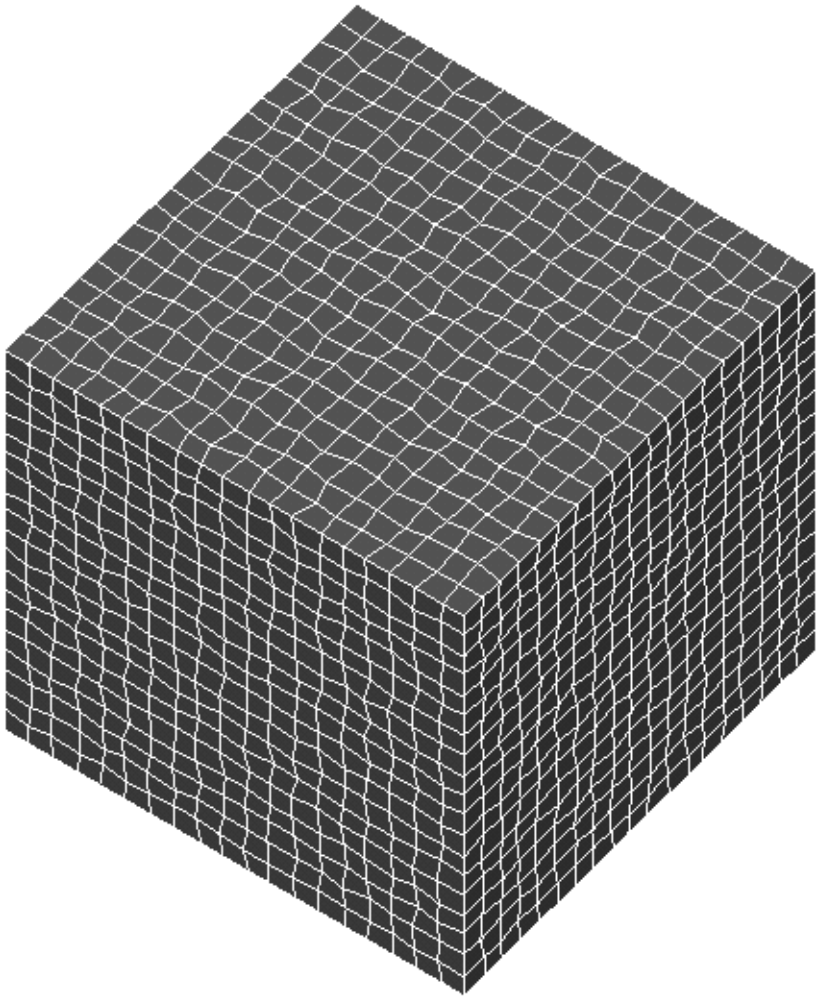

Figure 1: Wareing, McGhee, Morel and Pautz, “Cube of “Random” Non-Orthongonal Hexadedral Elements.”

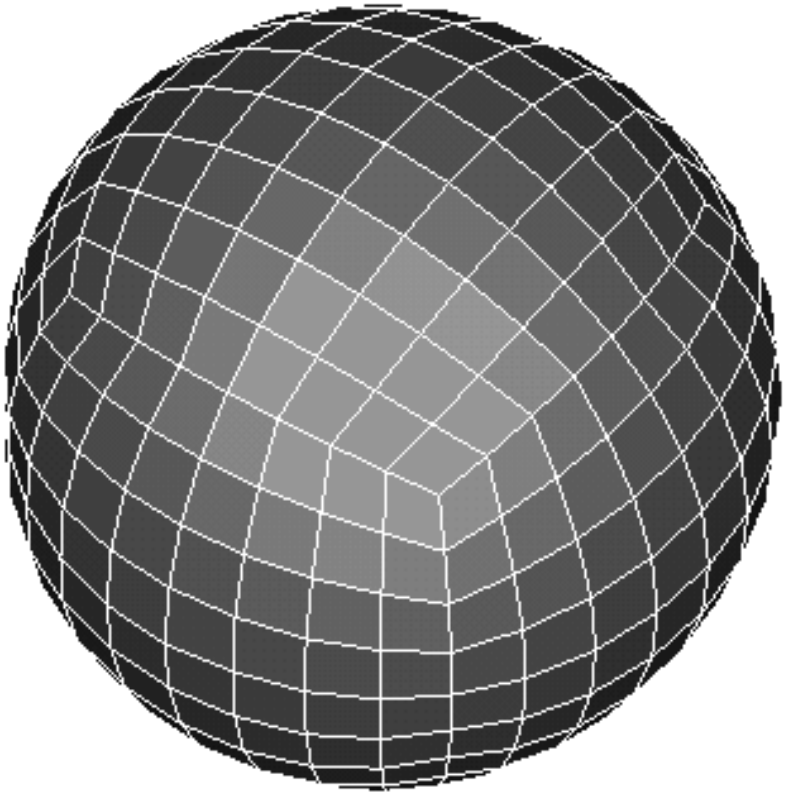

Figure 2: Wareing, McGhee, Morel and Pautz, “Sphere of Non-Orthongonal Hexadedral Elements.”

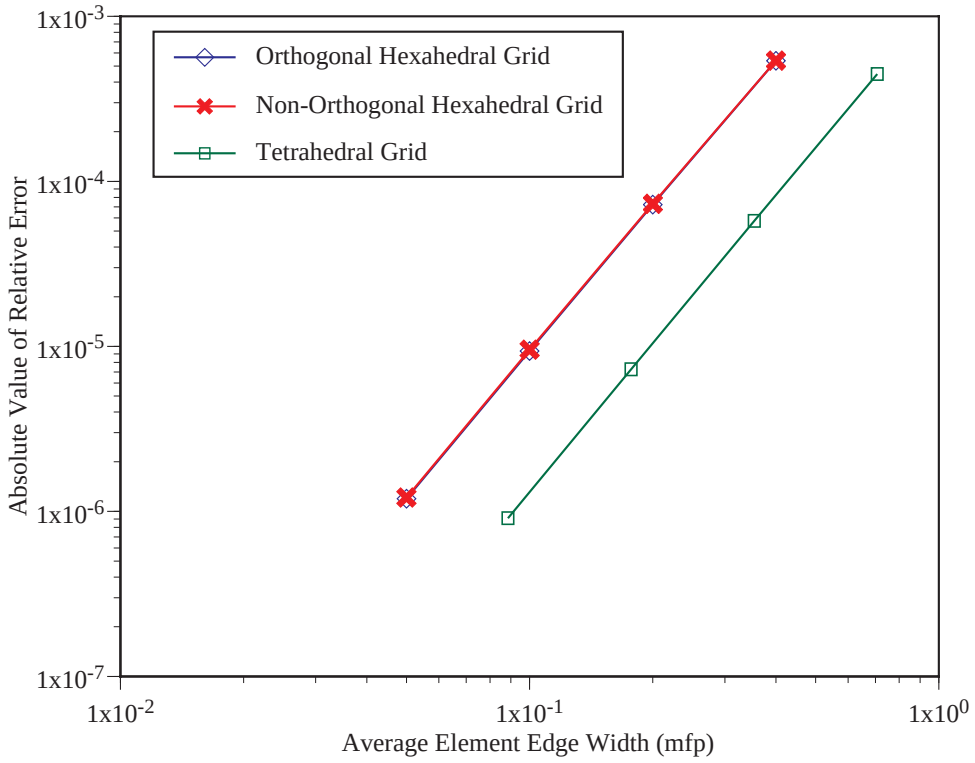

Figure 3: Wareing, McGhee, Morel and Pautz, “Absolute Error in Absorption Rate for Test Problem One.”

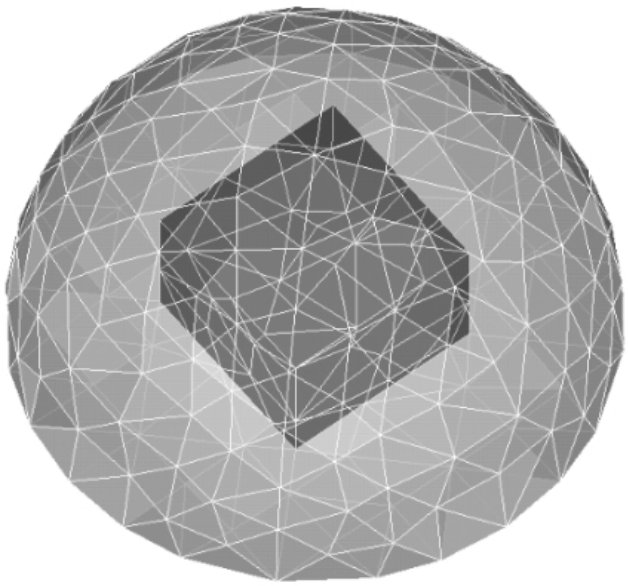

Figure 4: Wareing, McGhee, Morel and Pautz, “Tetrahedral Mesh For Test Problem Three.”

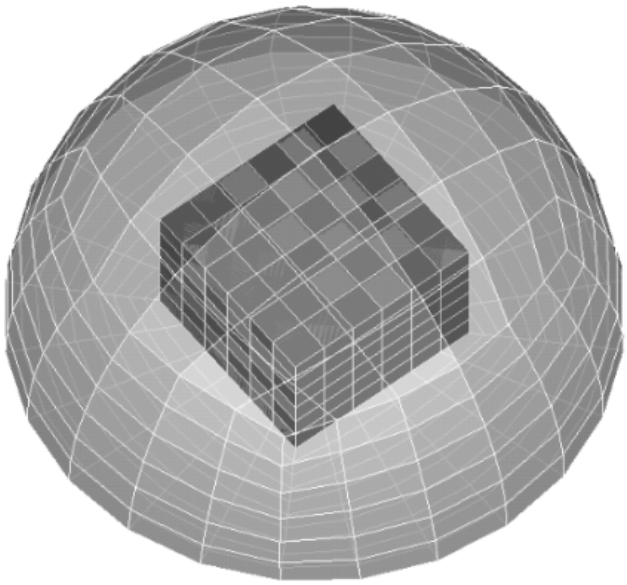

Figure 5: “Hexahedral Mesh For Test Problem Three.”